Supporting Information

Kim et al. 10.1073/pnas.1200081109

SI Materials and Methods

Cell Lines and Primary Tumors. Diffuse large B-cell lymphoma (DLBCL) cell lines were cultures at 37 °C in 5% CO_2 in RPMI-1640 medium (Invitrogen) containing 10% (vol/vol) (for Ly7, Ly8, Ly19, and DHL7) or 20% (vol/vol) (DHL2 and Ly10) FBS (or human serum), penicillin (100 units/mL), streptomycin (100 μg/mL), Hepes buffer (10 mmol/L), and L-glutamine (600 μg/mL). HEK-293 cells were maintained in Dulbecco's modified Eagle media (DMEM; Mediatech) with 10% FBS and sodium pyruvate (1 mmol/L). Eighteen well-characterized primary DLBCL samples were obtained from our local tumor bank. The clinical, pathological, and molecular features of this collection have been described previously (1) and are summarized in Table S1. These studies were approved by the institutional review board of the University of Texas Health Science Center at San Antonio.

Antibodies. IκBα (sc-371; Santa Cruz Biotechnology), p65/RelA (sc-372; Santa Cruz Biotechnology), phospho-IκBα (9246; Cell Signaling Technology), TNFAIP3 (60-6629-82; eBioscience), RIP1 (H-207; Santa Cruz Biotechnology), RIP1 (38; BD Biosciences Pharmingen), TRAF2 (C20; Santa Cruz Biotechnology), K63-linkage ubiquitin (PW0600; Enzo Life Sciences), BLIMP-1 (9115; Cell Signaling Technology) IRF-4 (4948; Cell Signaling Technology), FLAG (M2 clone; Sigma), histone H3 (4499; Cell Signaling Technology), Ago2/eIF2C2 (ab57113; Abcam), β-actin (A2228; Sigma-Aldrich). Histone H3 and β-actin were used as protein loading controls.

Cloning and Mutagenesis of miR-125a/b Binding Sites in TNFAIP3's Coding Region and 3′-UTR. These reporter constructs were generated in two steps. First, a coding-region fragment containing the miR-125a/b binding site was generated by PCR and cloned into the pMIR luciferase vector (Ambion) using SpeI and MluI cloning sites. Next, site-directed mutagenesis was performed, introducing three mutations into the binding site's seed sequence (shown in italic below). Subsequently, a DNA fragment containing the 3′-UTR miR-125a/b binding site was generated by PCR and cloned into pMIR vector, this time using MluI and HindIII sites. Again, site-directed mutagenesis was used to change all six nucleotides within the seed sequence (shown in bold below). Finally, WT or mutant 3′-UTR fragments were subcloned into the coding-region constructs (WT or mutant) using MluI and HindIII, resulting in WT/WT, WT/Mut, Mut/WT, Mut/Mut constructs. All constructs were sequenced to confirm their identity. The primers used for PCR amplification and mutagenesis are underlined; nucleotides within the seed sequence that were mutated are shown in italic and bold fonts.

TNFAIP3 coding region.

cgactagtCCAGCGTTCCAAGTCAGATCCCTCGCGGCTCG-TCCGGAGCCCCTCCCCGCATTCTTGCCACAGAGCTG-GAAACGACGCCCCTGCTGGCTGCCTGTCTCAAGCT-GCACGGACTCCTGGGGACAGGACGGGGACGAGCA-AGTGCAGAAAAGCCGGCTGCGTGTATTTTGGGAC-TCCAGAAAACAAGGGCTTTTGCACACTGTGTTTCA-TCGAGTACAGAGAAAACAAACATTTTGCTGCTGCC-TCAGGGAAAGTCAGTCCCACAGCGTCCAGGTTCCAG-AACACCATTCCGTGCCTGGGGAGGGAATGCGGCAC-CCTTGGAAGCACCATGTTTGAAGGATACTGCCAGA-AGTGTTTCATTGAAGCTCAGAATCAGAGATTTCATG-AGGCCAAAAGGACAGAAGAGCAACTGAGATCGAG-acgcgtcg.

TNFAIP3 3′-UTR.

ccacgcgtCATCGTCTTGGCTGAGAAAGGGAAAAGACA-CACAAGTCGCGTGGGTTGGAGAAGCCAGAGCCATT-CCACCTCCCCTCCCCCAGCATCTCTCAGAGATGTGAA-GCCAGATCCTCATGGCAGCGAGGCCCTCTGCAAGAA-GCTCAAGGAAGC**TCAGGG**AAAATGGACGTATTCAGA-GAGTGTTTGTAGTTCATGGTTTTTCCCTACCTGCCC-GGTTCCTTTCCTGAGGACCCGGCAGAAATGCAGAA-CCATCCATGGACTGTGATTCTGAGGCTGCTGAGAC-TGAACATGaagcttcg.

Reporter Assays. The constructs described above were cotransfected in HEK-293 cells with the pCMVβ-gal plasmid and 50 nM each of chemically synthesized pre–miR-125a, pre–miR-125b or pre–miR negative control oligonucleotides (Applied Biosystems), as we reported (2). Cells were harvested 48 h after transfection, and luciferase and β-galactosidase activities measured. Statistical significance of the differences in luciferase activity was determined by Student's *t* test.

Stable or Transient Modulation of miR-125a and miR-125b Levels in DLBCL Cell Lines. To create DLBCL cell lines (Ly7, Ly8, Ly19, and DHL2) stably expressing miR-125a or miR-125b (125b1 locus on chromosome 11q23), fragments of ∼400 bp encompassing their respective precursor miRNA sequences were PCR amplified and cloned into the MSCV–eGPP retrovirus vector. Virus production, transduction, and enrichment of $eGFP^+$ cells were performed as we described (2). Knockdown of miRNA expression in the DLBCL cell lines DHL7 and Ly10 was performed by transiently transfecting single-stranded anti–miR-125a, anti–miR-125b, or control anti–miR oligonucleotides (Applied Biosystems), as we described (2). Mature miR-125a or -125b expression in these genetically modified cells and their isogenic controls was determined with a stem-loop real-time RT-PCR strategy (TaqMan MicroRNA assay; Applied Biosystems).

Generation of miR-125 Refractory FLAG-Tagged TNFAIP3 Construct. A wild-type TNFAIP3 cDNA construct, lacking 3′-UTR, was generated by RT-PCR and introduced into MSCV–puromycin retrovirus using BglII and XhoI cloning sites. The FLAG-tag sequence was included in the 3′ oligonucleotide and incorporated in the cDNA by the PCR. To abolish the miR-125a/b binding site (seed sequence TCAGGG, amino acids 641–642), site-directed mutagenesis was used, modifying TCA (Ser) to AGT (Ser). The final construct was sequence verified.

Cloning primers. Restriction sites are underlined and in bold. FLAG sequence is underlined.

5′ GACTC**AGATCT**ATGGCTGAACAAGTCCTTCCTCA-GGCTTTGTATTTGAGC 3′

5′ CC**GTCGAC**TTACTT GTC GTC ATC GTC TTT GTA GTC GCCATACATCTGCTTG 3′.

Mutagenesis primers. Mutated nucleotides as shown in small caps, mutant seed sequence is underlined. 5′ CAA ACA TTT TGC TGC T GCC agt GGG AAA GTC AG TCC CAC AGC G

5′ CGC TGT GGG ACT GAC TTT CCC act GGC AGC AGC AAA ATG TTT G.

Stable Reconstitution of TNFAIP3 Expression in DLBCL Cells. Ly7 cells stably expressing miR-125a and miR-125b were transduced with MSCV–puromycin or MSCV puromycin–TNFAIP3–FLAG vi-

ruses. Stable clones were obtained by puromycin selection, and ectopic TNFAIP3 expression was confirmed by anti-FLAG Western blotting.

Subcellular Fractionation and Immunoblotting. Genetically modified Ly7, Ly8, and Ly19 cells were starved overnight in 2% FBS media, exposed to TNFα (PeproTech) or vehicle for various time points. Electrophoresis of whole cell lysates (from cell lines or primary tumors), cytoplasmic, and nuclear protein fractions were performed as we described (2) and expression of relevant proteins were detected with specific antibodies. Histone H3 and β-actin were used as protein loading controls.

Expression of NF-κB Target Genes and NF-κB Activity Assay. RNA was isolated and cDNA synthesized, as we previously described (1, 2). Expression of the NF-κB transcriptional targets *CD83, BIRC3, NFKB2, TNF, IRF1*, and *TNIP1* was determined by quantitative real-time RT-PCR in DLBCL cell lines stably expressing miR-125a, miR-125b, or empty MSCV vector following exposure to TNFα (200 ng/mL for 120 min) or vehicle control (primers sequences are listed below). Statistical significance ($P < 0.05$) of the differences in expression was determined by Student's *t* test. Quantification of all genes was performed in triplicate. The DNA-binding activity of p65 was examined in protein extracts of DLBCL cell lines with stable or transient genetic modification of miR-125a and miR-125b expression, as well as primary DLBCL biopsies, according to the manufacturer's instructions (TransAM p65 kit; Active Motif). DLBCL cell lines measurements were performed in triplicate and repeated three times; primary DLBCL samples were examined in duplicate. Statistical significance ($P < 0.05$) of the differences in NF-κB activity was determined by Student's *t* test.

Immunoprecipitation and Ubiquitination of RIP1 and TRAF2s. Ly8–MSCV, Ly8–miR-125a, and Ly8–miR-125b were starved overnight in serum-free media, exposed to 100 ng/mL of TNFα or vehicle for multiple intervals, and whole cell lysates harvested in RIPA buffer supplemented with the cysteine protease inhibitor *N*-ethylmaleimide (Sigma). Lysates were immunoprecipitated with IgG control, RIP1, or TRAF2 antibodies, and the ubiquitination levels detected with an antibody to K63 linkage-specific ubiquitin. Equal immunoprecipitation/loading was determined by reprobing with RIP1 or TRAF2 antibodies, whereas IgG control confirms the specificity of the procedure. Quantification of the input RIP1 and TRAF2 was determined by Western blotting, and the kinetics of the NF-κB activation was defined by the phospho and total levels of IκBα (Fig. S5).

Immunoprecipitation of AGO2-Containing RNA-Induced Silencing Complex (RISC). Ly8–MSCV, Ly8–miR-125a, and Ly8–miR-125b were washed once with PBS and lysed for 30 min in buffer containing 25 mM Tris-HCl, pH 7.4, 150 mM KCl, 5 mM EDTA, 0.5% Nonidet P-40, 5 mM DTT, protease inhibitors, and 100 units/mL of RNasin Plus (Promega), as described (3, 4). To form the Ago2/anti-Ago2 antibody complexes, 1 mg of lysate was incubated with 5 μg of anti-Ago2 antibody or normal mouse IgG for 3 h, followed by 50 μL of A/G agarose beads for 2 h. Subsequently, the immunocomplexes were washed three times and used for RNA isolation (9/10 of the IP) or immunoblots (1/10 of the IP). cDNA was synthesized with 50 ng of RNA using SuperScript VILO cDNA synthesis kit (Invitrogen) and quantitative real-time RT-PCR was performed to determine *TNFAIP3* enrichment in the RISC; RISC-associated *GAPDH* was used for normalization, as described (3).

Cell Growth, Soft Agar Colony-Forming Assays, and Apoptosis Assays. Multiple DLBCL cell lines genetically modified to express miR-125a and miR-125b were plated at 5×10^5/mL in RPMI media supplemented with 10% (Ly7, Ly8, and Ly19) or 20% (DHL2) and cell numbers counted daily with a trypan blue exclusion assay. All experiments were performed in triplicate and repeated at least three times. Colony-forming assays were performed in triplicate by embedding 2×10^4 to 5×10^5 cells in 2.5 mL of fully supplemented RPMI media, and 0.4% low melting agarose (OmniPur) in 12-well plates. Colonies were counted and photographed 10–21 d later. All assays were repeated at least two times. Apoptosis was measured in response to oxidative or starvation stresses using a propidium iodide (PI) (P4170; Sigma) flow cytometric assay, as we described (2). In brief, DLBCL cell lines genetically modified to express miR-125a, miR-125b, or their isogenic controls were exposed to increasing doses of hydrogen peroxide or starved in serum-free conditions (Ly8, Ly19, and DHL2) or 2% serum (Ly7). At multiple time points, cells were harvested, fixed in cold 70% ethanol, stained with PI, and analyzed by flow cytometry on a LSRII (Becton-Dickinson) instrument using the BD FACS Diva software.

PCR Amplification and Sequencing of CARD11, MYD88, CD79B, and TNFAIP3. Genomic DNA was isolated from 18 primary DLBCLs and PCR fragments subjected to Sanger sequencing. All mutations were confirmed on independent PCR products. Primer sequences are listed below.

Gain or Loss of Genetic Material Targeting miR-125a and miR-125b Loci. The genomic analysis of the miR-125a/b loci in DLBCL patients was performed earlier as part of a larger study that evaluated the integrity of ~470 miRNA genes in these tumors; please refer to ref. 1 for further details. In brief, we used the eArray interface (Agilent Technologies) to create a miRNA specific array-comparative genomic hybridization (CGH) platform. In this design, the genomic coordinates from 474 miRNA genes were extracted and used to search for all oligonucleotide probes available in the Agilent catalog located within a ~35-kb area surrounding each precursor miRNA sequence. These high-density tilling arrays included 41,631 oligoprobes (~55 bp long, 44–59 bp) with a total genomic coverage of 11.6 Mb that specifically targeted the miRNA loci in 309 unique chromosomal regions. The array-CGH data were analyzed using dChip software. To obtain the miRNA gene copy number, we first organized the probes into miRNA regions. The log2 ratio values of all of the probes in a region were averaged to obtain the miRNA region-level log2 ratios, and copy number summary plots were used to determine the proportion of the samples that had copy number gains (copy ≥2.5) or losses (copy ≤1.5).

Primers Used for Real-Time RT-PCR Measurement of NF-κB Target Genes.

TNF-F 5′ AGGGACCTCTCTCTAATCAG 3′
TNF-R 5′ TGGGAGTAGATGAGGTACAG 3′
TNIP1-F 5′ TTTGCAGAAGCAGGTGACTG 3′
TNIP1-R 5′ TTTTCCTGGTACTCACGCTG 3′
IRF1-F 5′ GCACCAGTGATCTGTACAAC 3′
IRF1-R 5′ GCTCCTCCTTACAGCTAAAG 3′
BIRC3-F 5′ TGTGATTAATGCTGCCGTGG 3′
BIRC3-R 5′ GTGCCATTCTATTCTTCCGG 3′
CD83-F 5′ CAGCACTATCATCAGAAGGG 3′
CD83-R 5′ AAATAACCAGAGCCAGCAGC 3′
NFKB2-F 5′ GAGACATGGAGAGTTGCTAC 3′
NFKB2-R 5′ GCCTTCACAGCCATATCGAA 3′.

Sequencing Primers.

CARD11: ex5-F 5′gagtgaatgaatggcacctg3′, ex5-R 5′cctggtgacatttgtttccc3′; ex6-F 5′ggtttcttggagcccttctc3′, ex6-R 5′atgcctgtgatcctgcagtc3′; ex8-F 5′gcagagaacagctttcagtc3′, ex8-R 5′aacactctgaa-

ggagccggtg3′; and ex9-F 5′ggctctgtgatcgcgttaatg3′, ex9-R 5′cttcaggtgtgggtctcca 3′.

MYD88: ex2-F 5′tgtgggtaaagaggtaggcac3′, ex2-R 5′cagcccatctgcttcaaacac3′; ex3-F 5′aagccttcccatggagctctgaccac3′, ex3-R 5′gctaggaggagatgcccagtatctg3′; ex4-F 5′actaagttgccacaggacctgcagc3′, ex4-R 5′atccagaggccccacctacacattc3′; and ex5-F 5′gttgaagactgggcttgtcc3′, ex5-R 5′gcacagattcctcctacaac3′.

CD79B: ex5/6-F 5′gcagaatgcacctcactcctg3′, ex5/6-R 5′agctccgaagcagtcactgag3′.

TNFAIP3: ex2-F 5′ggagtcgtattaaagtcaggctaa3′, ex2-R 5′ggcaaaagaaacacaacagaac3′; ex4-F 5′gggagtacaggatacattcaagc3′, ex4-R 5′gctgaaagcatttaagtacagatcc3′; ex7.1-F 5′ggttctacaattcttgccataatcc3′, ex7.1-R 5′caagtgccttgtgtggtctg3′; and ex7.2-F 5′cacaacggattttgtggaacg3′, ex7.2-R 5′aggaacaaaaccccttctgg3′.

1. Li C, et al. (2009) Copy number abnormalities, MYC activity, and the genetic fingerprint of normal B cells mechanistically define the microRNA profile of diffuse large B-cell lymphoma. *Blood* 113:6681–6690.
2. Rai D, Kim SW, McKeller MR, Dahia PL, Aguiar RC (2010) Targeting of SMAD5 links microRNA-155 to the TGF-beta pathway and lymphomagenesis. *Proc Natl Acad Sci USA* 107:3111–3116.
3. Fasanaro P, et al. (2009) An integrated approach for experimental target identification of hypoxia-induced miR-210. *J Biol Chem* 284:35134–35143.
4. Glorian V, et al. (2011) HuR-dependent loading of miRNA RISC to the mRNA encoding the Ras-related small GTPase RhoB controls its translation during UV-induced apoptosis. *Cell Death Differ* 18:1692–1701.

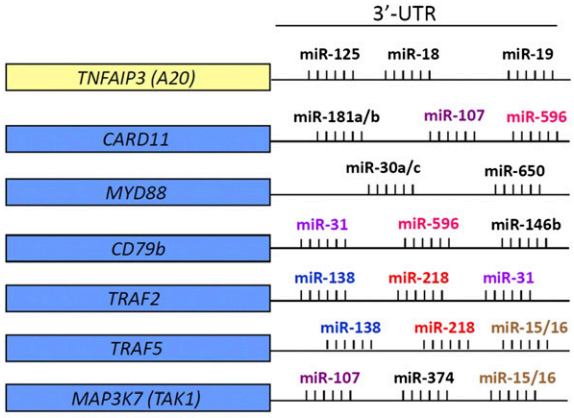

mRNA target	MiRNA ID	Gain	Loss
TNFAIP3	miR-125a/b1-b2	16.4%	
TNFAIP3	miR-18a/19a/b1	24.7%	
CARD11/CD79b	miR-596		13.7%
CARD11/TAK1/RANK	miR-107		9.6%
CARD11	miR-181a1/b1		4.1%
MYD88	miR-30a/c		8.2%
MYD88	miR-650		31.5%
CD79b/TRAF2	miR-31		17.8%
CD79b	miR-146b		4.1%
TRAF2/TRAF5	miR-218-1		6.8%
TRAF2/TRAF5	miR-138-2		4.1%
TRAF5/TAK1	miR-15a/16-1		13.7%
TAK1	MiR-374		6.8%

Fig. S1. Integration of a map of the miRNA genome with target gene prediction algorithms. We used TargetScan to search for microRNAs that may bind to regulators of the NF-κB previously shown to be mutated in DLBCL. We filtered the initial group of putatively relevant microRNAs, to enrich for those (*i*) that are known to be expressed in B lymphocytes (1, 2), (*ii*) that we showed to have copy number defects in DLBCL (3), (*iii*) that preferentially target more than one mRNA of interest and, (*iv*) that had the highest prediction scores. The interactions that survived this annotated screening are shown in the diagram (*Upper*), whereas the copy number changes that we reported earlier to target these loci in DLBCL (3) are listed in the table (*Lower*). MiRNAs predicted to target the tumor suppressor gene TNFAIP3 are amplified/overexpressed in DLBCL, whereas those potentially inhibiting genes with gain-of-function mutation in DLBCL are more often deleted. Color-coded miRNAs are predicted to target more than one gene in this pathway.

1. Basso K, et al. (2009) Identification of the human mature B cell miRNome. *Immunity* 30:744–752.
2. Zhang J, et al. (2009) Patterns of microRNA expression characterize stages of human B-cell differentiation. *Blood* 113:4586–4594.
3. Li C, et al. (2009) Copy number abnormalities, MYC activity, and the genetic fingerprint of normal B cells mechanistically define the microRNA profile of diffuse large B-cell lymphoma. *Blood* 113:6681–6690.

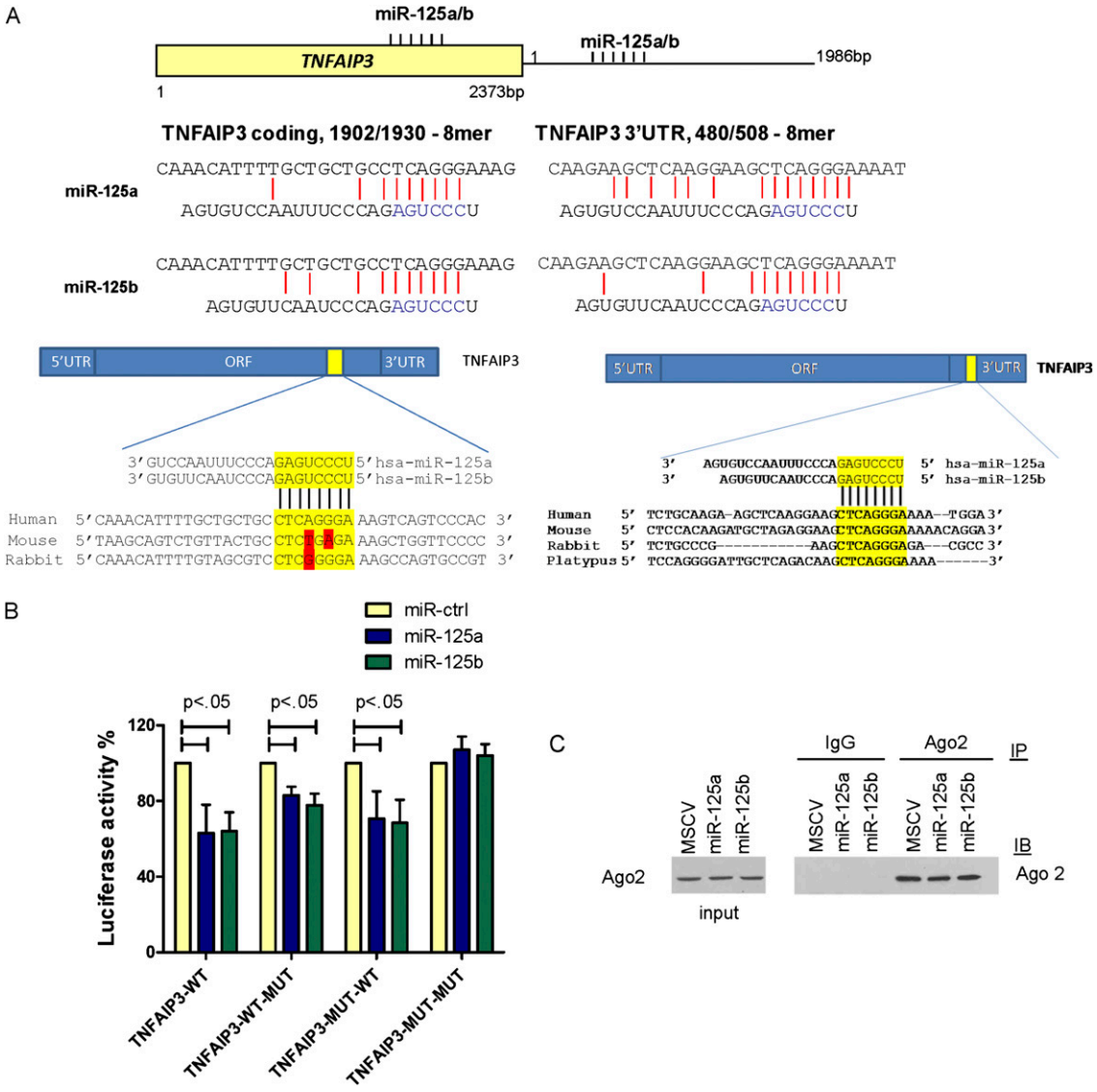

Fig. S2. Two functional sites mediate miR-125a and miR-125b targeting of TNFAIP3. (*A*) Diagrammatic representation of *TNFAIP3* gene structure and the location of the two functional miR-125a/b binding sites, which are detailed in the *Middle* panels; the 3′-UTR site is fully conserved, whereas the coding region site is not. (*B*) Luciferase reporter assays show that both binding sites are functional. Note that a construct with at least one WT seed sequence is suppressed by expression of miR-125a or miR-125b, albeit to a lesser extent than when both sites are in a WT configuration. However, when both the 3′-UTR and coding region sequences are mutated, the miRNAs lose their inhibitory effects. Data shown are mean ± SD of the ratio of luciferase activity (miR-125a or miR-125b vs. control oligo) of a representative assay; experiments were performed in triplicate and repeated three times. (*C*) Western blot analysis of immunoprecipitation of AGO2-containing RISC (*Right*) and input protein (*Left*), demonstrate equal pulldown and expression of this protein in isogenic cells expression MSCV-only, miR-125a, or miR-125b. IgG control confirms the specificity of the IP.

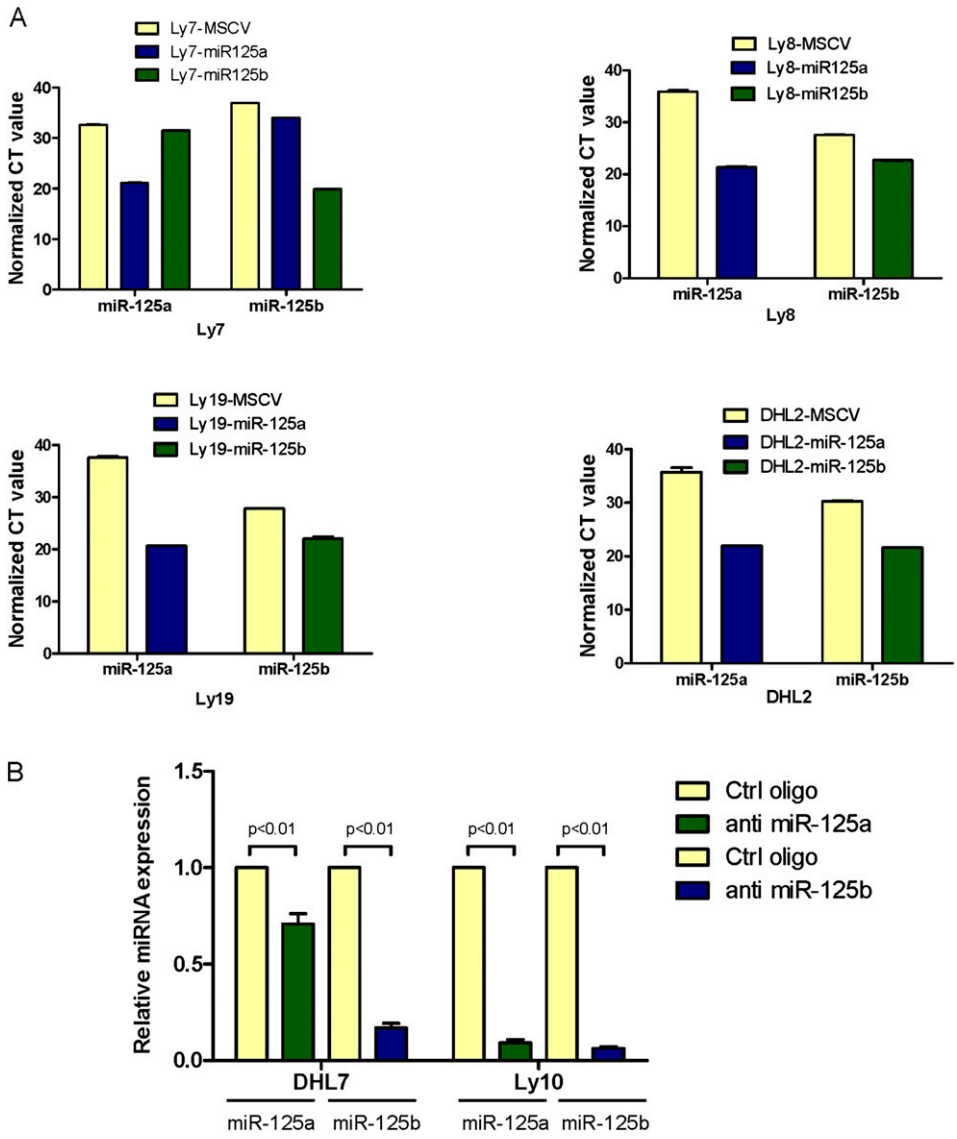

Fig. S3. Expression of miR-125a and miR-125b in genetically modified DLBCL cell lines. (*A*) Stable integration of MSCV–125a or MSCV–miR125b retrovirus constructs markedly elevated the expression of these miRNAs in four independent DLBCL cell lines. The data are displayed as CT value normalized by U18 expression; thus, the lower the CT value, the higher the expression. The specificity of this genetic modulation, and its measurements, is shown in Ly7 (*Upper Left*), where ectopic expression of miR-125a does not change miR-125b levels and vice versa. In all cell lines, irrespective of the endogenous levels of miR-125a or miR-125b, MSCV-driven ectopic expression resulted in comparable ectopic miRNA level (CT value ~20). (*B*) Transient transfection of miR-125a or miR-125b antagomirs significantly lowered these miRNAs expression in two DLBCL cell lines. All miRNAs quantifications were performed with the stem-loop RT-PCR assay (ABI) as we described (3, 4). Data shown are mean ± SD of triplicates; statistical significance of the differences was defined by Student's *t* test.

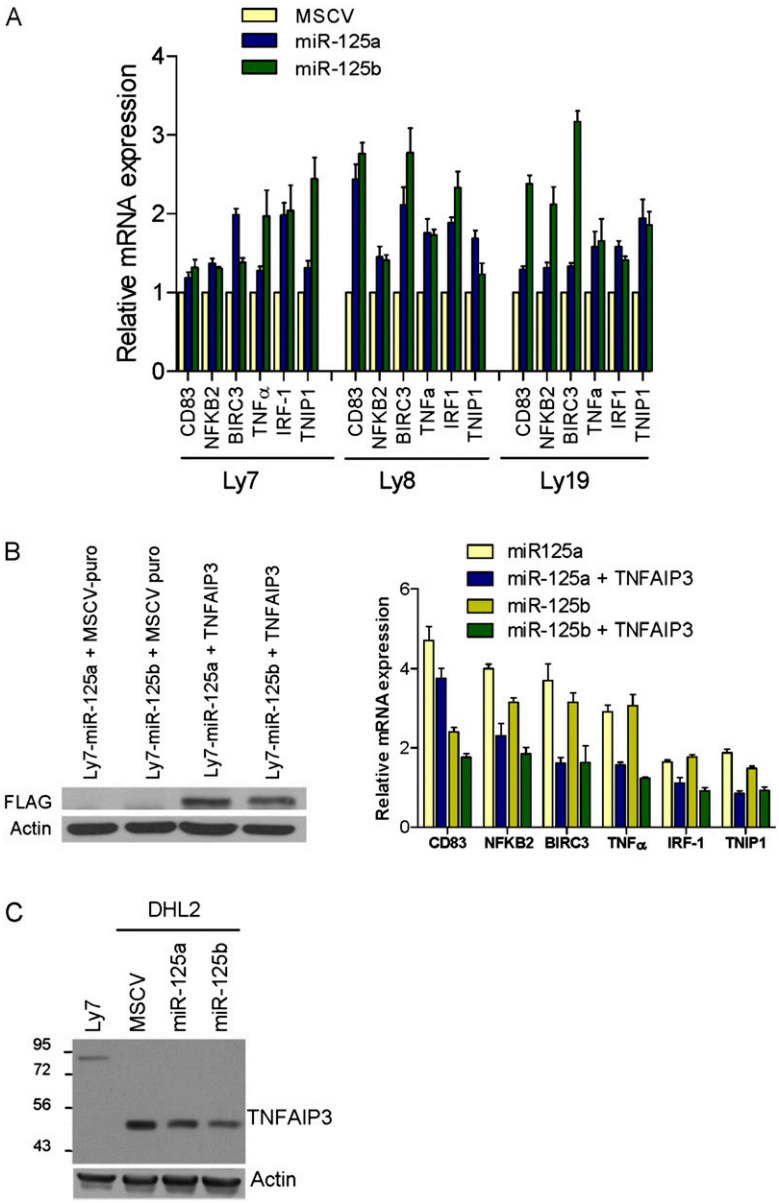

Fig. S4. Aberrant induction of NF-κB target genes in DLBCL cell lines ectopically expressing miR-125a and miR-125b, or reconstituted with TNFAIP3. (*A*) Real-time RT-PCR of multiple NF-κB transcriptional targets shows that stable expression of miR-125a/b consistently elevates the expression of these genes. Data are mean ± SD of the mRNA fold induction following exposure to TNFα (200 ng/mL for 120 min), normalized by MSCV-only cells, of a representative experiment. The six genes selected for use in this study are readily inducible by TNFα stimulation in our cell models and are among the validated NF-κB target genes with relevance to the biology of normal and malignant B cells, as described in ref. 1. (*B*) A FLAG-tagged TNFAIP3 construct was stably expressed in the Ly7 DLBCL cells ectopically expressing miR-125a/b (*Left*). Real-time RT-PCR of NF-κB targets showed that reconstitution of TNFAIP3 rescued the miR-125a/b–induced effects, resulting in significantly lower expression of all six genes in FLAG–TNFAIP3 cells (*Right*). Assays in *A* and *B* were performed in triplicate and confirmed in three biological replicates. All of the observed differences are statistically significant ($P < 0.05$, Student's *t* test). (*C*) Western blot depiction of the wild-type and truncated TNFAIP3 isoforms in Ly7 (~88 kDa) and DHL2 (~50 kDa), respectively; this assay also confirms that miR-125a/b binding sites are intact in the mutant *TNFAIP3* mRNA, resulting in inhibition of the expression of this nonfunctional protein.

1. Feuerhake F, et al. (2005) NFkappaB activity, function, and target-gene signatures in primary mediastinal large B-cell lymphoma and diffuse large B-cell lymphoma subtypes. *Blood* 106: 1392–1399.

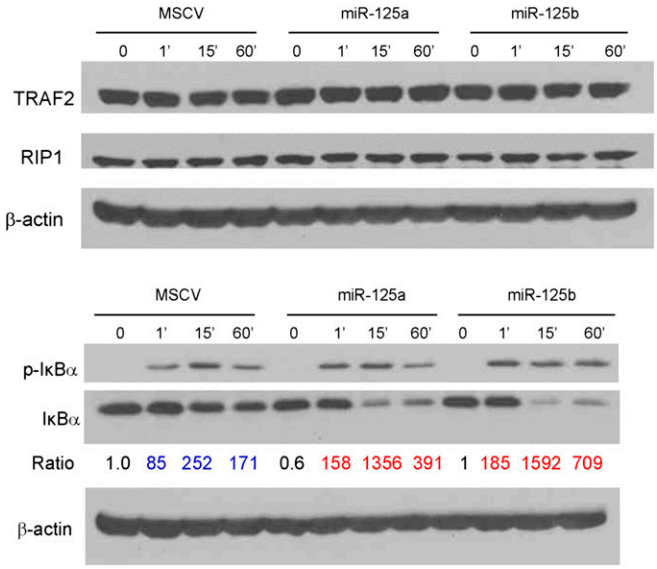

Fig. S5. MiR-125a and miR-125b expression modulate K63-linkage ubiquitination of TRAF2 and RIP1. *Upper* panels confirm equal expression of these proteins in the input lysates of isogenic Ly8 cells expressing empty MSCV, MSCV–miR-125a, or MSCV–miR-125b (used in IP shown in Fig. 3). *Lower* panels confirm that TNFα stimulation (100 ng/mL) induced NF-κB activation (phosphorylation and degradation of IkBα) in these cells, which as we show in Figs. 2 and 4 is more pronounced in miR-125a/b–expressing cells than in isogenic MSCV-only controls.

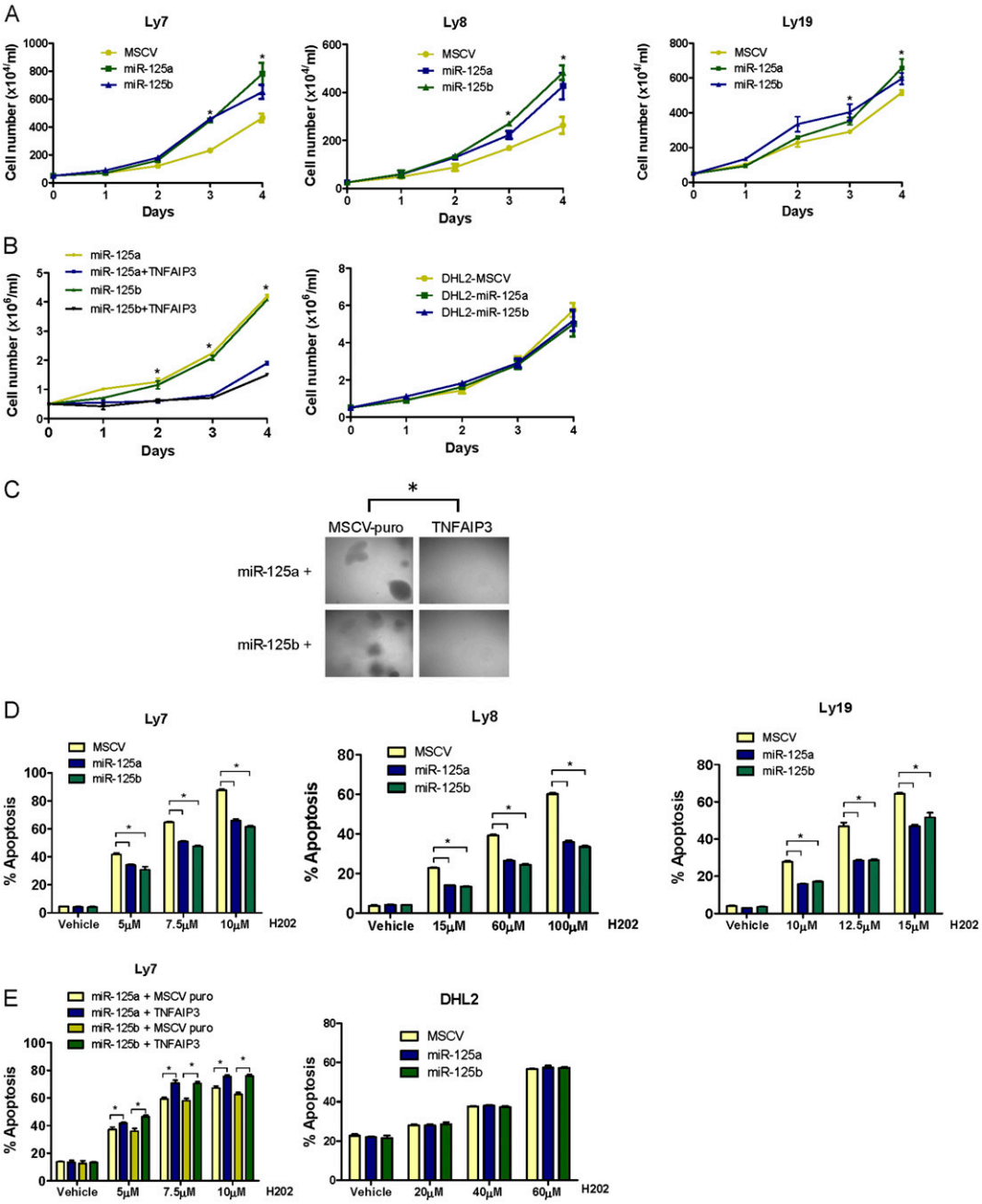

Fig. S6. MiR-125a and miR-125b enhance the aggressiveness of DLBCL cell lines in vitro. (*A*) DLBCL cell lines stably expressing miR-125a/b grow significantly faster than their empty vector isogenic controls. (*B*) Reconstitution of TNFAIP3 expression rescued the higher growth rate induced by miR-125a and miR-125b in DLBCL (*Left*), whereas ectopic expression of miR-125a/b had no effect in the growth of the TNFAIP3-null DLBCL cell line DHL2 (*Right*). In *A* and *B*, cells were plated at 5×10^5/mL in RPMI media supplemented with 10% (Ly7, Ly8, and Ly19) or 20% (DHL2) and cell numbers counted daily with a trypan blue exclusion method; all assays were performed in triplicate and repeated at least three times. (*C*) TNFAIP3 expression rescued the effects of stable miR-125a/b on colony formation in soft agar; cells coexpressing miR-125a or miR-125b and TNFAIP3 did not form colonies, in contrast to isogenic controls expressing miR-125a/miR-125b and an empty MSCV–puromycin vector. *$P < 0.05$, Student's *t* test. (*D*) Stable expression of miR-125a/b rendered multiple TNFAIP3-competent DLBCL cell lines resistant to apoptosis induced by H202. (*E*) Reconstitution of TNFAIP3 expression restored the H202-induced apoptotic response (*Left*), whereas stable expression of miR-125a/miR-125b did not modify the rate of H202-induced apoptosis in the TNFAIP3-null DLBCL cell line (*Right*). For all assays, data shown are mean ± SD of triplicates and repeated from two to four times; Ly7 data were collected at 48 h; all other cell lines at 72 h. *$P < 0.05$, Student's *t* test.

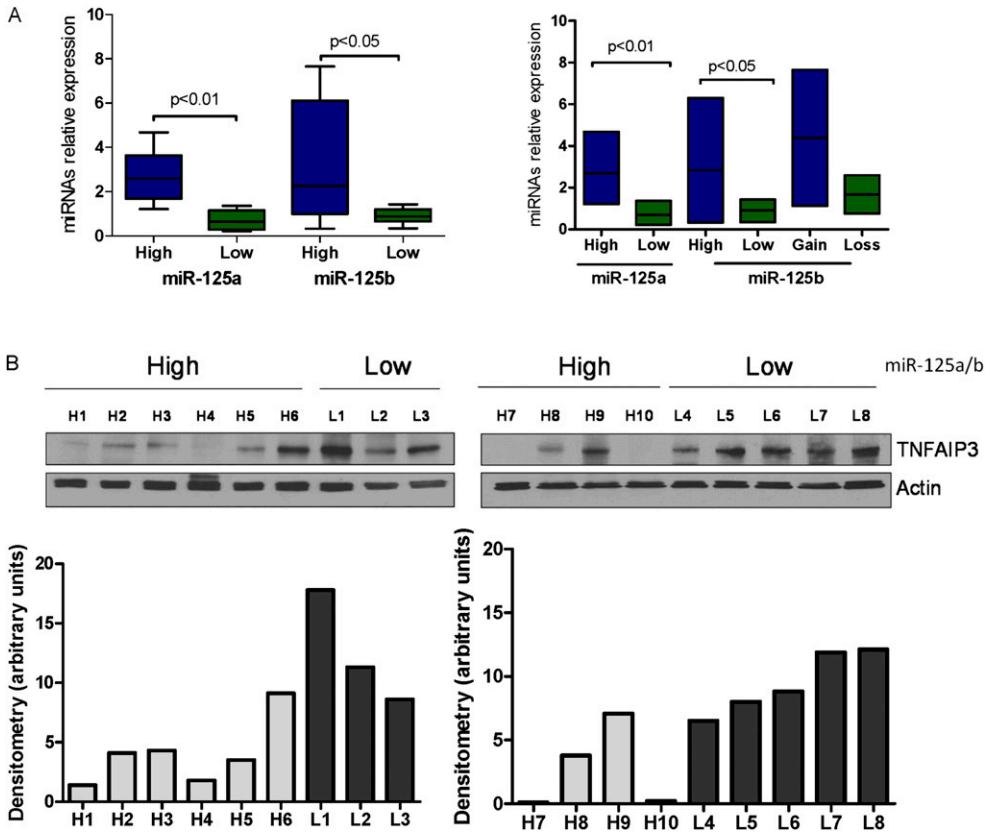

Fig. S7. Inverse correlation between miR-125a and miR-125b expression TNFAIP3 levels in primary DLBCL. (*A*, *Left*) Real-time stem-loop RT-PCR quantification of miR-125a and miR-125b was initially used to dichotomize our tumor cohort into two groups with statistically different expression of these miRNAs ($P < 0.05$, Student's *t* test). Data shown are mean ± SD of the miRNAs expression normalized by U18 and performed in triplicate. (*Right*) Four tumor samples with gain or loss of genetic material at the miR-125b1/2 loci are displayed independently. (*B*) Protein isolated from a cohort of 18 frozen DLBCL biopsies was subjected to SDS/PAGE electrophoresis and immunoblotted with an anti-TNFAIP3 antibody; β-actin was used as loading control. Densitometric quantification of TNFAIP3 expression (*Bottom*), normalized by β-actin levels, shows that this protein is significantly less abundant in DLBCLs with high (H) miR-125a and/or miR-125b expression than in those with low (L) levels of these miRNAs ($P < 0.01$, Mann–Whitney test).

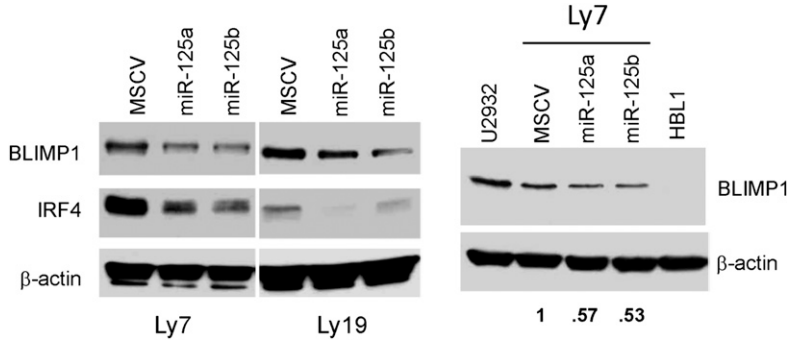

Fig. S8. MiR-125a and miR-125b–mediated inhibition of BLIMP1 and IRF4. BLIMP1 and IRF4 have been described as direct targets of miR-125b (1, 2). We used Western blotting to show that ectopic expression of miR-125b as well as miR-125a down-regulate these B-cell transcription factors in DLBCL cell lines. (*Right*) Specificity of the BLIMP1 detection is confirmed with the inclusion of positive and negative controls, the U2932 and HBL1 DLBCL cell lines, respectively, as reported in Mandelbaum et al. (3).

1. Chaudhuri AA, et al. (2011) MicroRNA-125b potentiates macrophage activation. *J Immunol* 187:5062–5068.
2. Gururajan M, et al. (2010) MicroRNA 125b inhibition of B cell differentiation in germinal centers. *Int Immunol* 22:583–592.
3. Mandelbaum J, et al. (2010) BLIMP1 is a tumor suppressor gene frequently disrupted in activated B cell-like diffuse large B cell lymphoma. *Cancer Cell* 18:568–579.

Table S1. Clinical, pathological, and molecular features of the primary DLBCLs included in this study

			Copy number				
Tumor ID	Diagnosis	COO	TNFAIP3	miR-125b1	miR-125b2	miR-125a	Mutation status
H1	DLBCL	GCB	Diploid	Gain (2.65)	Diploid (2.28)	Diploid (1.69)	WT
H2	DLBCL	GCB	Diploid	Diploid (1.97)	Diploid (1.94)	Diploid (2.02)	WT
H3	DLBCL	Non-GCB	Diploid	Gain (2.84)	Diploid (2.01)	Diploid (1.97)	WT
H4	DLBCL	GCB	ND	ND	ND	ND	WT
H5	DLBCL	GCB	Diploid	Diploid (2.07)	Hemizygous loss (1.42)	Diploid (2.28)	WT
H6	DLBCL	Non-GCB	ND	ND	ND	ND	MYD88,S243N; CD79B, Y196D
H7	DLBCL	Non-GCB	Diploid	Diploid (1.88)	Diploid (1.83)	Diploid (2.41)	WT
H8	DLBCL	GCB	ND	ND	ND	ND	MYD88, L265P
H9	DLBCL	GCB	Diploid	Diploid (2.00)	Diploid (2.11)	Diploid (2.03)	WT
H10	DLBCL	GCB	ND	ND	ND	ND	WT
L1	DLBCL	Non-GCB	Diploid	Diploid (2.00)	Diploid (2.05)	Diploid (2.05)	WT
L2	DLBCL	Non-GCB	Diploid	Diploid (1.75)	Diploid (1.78)	Diploid (1.94)	TNFAIP3, (G/C,-1) splice site, ex4
L3	DLBCL	GCB	Diploid	Hemizygous loss (1.4)	Diploid (2.04)	Diploid (2.08)	WT
L4	DLBCL	Non-GCB	Diploid	Diploid (2.05)	Diploid (2.13)	Diploid (1.99)	TNFAIP3, C608X
L5	DLBCL	GCB	ND	ND	ND	ND	WT
L6	DLBCL	GCB	Diploid	Diploid (2.38)	Diploid (2.13)	Diploid (1.97)	WT
L7	DLBCL	Non-GCB	Diploid	Diploid (2.23)	Diploid (1.85)	Diploid (2.31)	WT
L8	DLBCL	Non-GCB	Hemizygous loss	Diploid (2.27)	Diploid (1.65)	Diploid (1.79)	WT

COO, cell-of-origin defined by immunohistochemistry based on the algorithm in ref. 1. Copy number, gain (copy $\geq$2.5) and loss (copy $\leq$1.5), as described in ref. 2. Mutation status, CARD11, MYD88, TNFAIP3, and CD79B. ND, not determined.

1. Hans CP, et al. (2004) Confirmation of the molecular classification of diffuse large B-cell lymphoma by immunohistochemistry using a tissue microarray. *Blood* 103:275–282.
2. Li C, et al. (2009) Copy number abnormalities, MYC activity, and the genetic fingerprint of normal B cells mechanistically define the microRNA profile of diffuse large B-cell lymphoma. *Blood* 113:6681–6690.